Acta Crystallographica Section B
Structural Science, Crystal Engineering and Materials
ISSN 2052-5192

Structure determination of the crystalline phase of *n*-butanol by powder X-ray diffraction and study of intermolecular associations by Raman spectroscopy

Patrick Derollez,* Alain Hédoux, Yannick Guinet, Florence Danède and Laurent Paccou

Unité Matériaux et Transformations (UMR CNRS 8207), Université Lille 1, Sciences et Technologies, Villeneuve d'Ascq CEDEX 59655, France

Correspondence e-mail: patrick.derollez@univ-lille1.fr

Received 13 September 2012
Accepted 19 February 2013

X-ray powder diffraction patterns of *n*-butanol at 110 K and the isothermal transformation above the glass transition temperature of the supercooled liquid into the glacial state were recorded with a laboratory diffractometer. The starting structural model of the crystalline stable phase was found by a Monte-Carlo simulated annealing method. The final structure was obtained through Rietveld refinements with soft restraints on the interatomic bond lengths and angles. The cell is triclinic with space group $P1$ and contains two molecules. The width of the Bragg peaks is interpreted by a phenomenological microstructural approach in terms of anisotropic strain effects. The study of the hydrogen bonds by Raman spectroscopy shows the existence of two main kinds of hydrogen bonds in the crystal, in agreement with the structure obtained by diffraction. The glacial state resulting from an abortive crystallization is composed of microcrystallites of the stable phase coexisting with non-transformed supercooled liquid. Crystalline features of the glacial state were determined as closely connected to the microstructural description of the crystal, leading to information about the origin of the glacial state.

1. Introduction

Polyamorphic transitions and the related glass-transition mechanisms have attracted great attention since the identification of a first-order transition between two amorphous states in ice (Mishima *et al.*, 1985). More recently, the detection of a second apparently amorphous state, referred to as the *glacial state*, in triphenyl phosphite (TPP; Ha *et al.*, 1996; Cohen *et al.*, 1996) and *n*-butanol (Bolshakov & Dzhonson, 2005; Kurita & Tanaka, 2005), under atmospheric pressure and at accessible low-temperatures using liquid nitrogen devices, has extended experimental investigations in the field of molecular glass-forming systems. On the basis of Raman, X-ray diffraction and thermodynamic investigations on TPP (Hédoux *et al.*, 1998, 2004, 2006; Derollez *et al.*, 2004; Hernandez *et al.*, 2002) and *n*-butanol (Wypych *et al.*, 2007; Shmyt'ko *et al.*, 2010), it was shown that the apparently second amorphous state was a nano-/microcrystalline state resulting from an abortive crystallization process. A detailed structural analysis of glacial and crystalline TPP (Hernandez *et al.*, 2002; Derollez *et al.*, 2004, 2006) has shown that the glacial state could be interpreted as a heavily nucleated state composed of micro- or nanocrystals of the stable crystalline phase. The frustration responsible for the abortive crystallization was determined as being the consequence of a very high nucleation rate in a temperature range where the growth rate is low (Hédoux *et al.*, 2004). Raman investigations on *n*-butanol have suggested that the origin of the frustration of crystallization

was related to the rearrangement of hydrogen-bonded molecules (Wypych *et al.*, 2007). It was shown that linear chains of approximately ten molecules exist in the liquid state *via* the analysis of the prepeak, considered as the signature of correlations between hydrogen-bonded alcohol molecules (Vahvaselkä *et al.*, 1995). The connection between these molecular associations and structural heterogeneities suspected to be involved in the slowing down of the dynamics approaching the glass transition (Adam & Gibbs, 1965; Kivelson *et al.*, 1995) is still unclear. Raman spectroscopy investigations (Wypych *et al.*, 2007) have revealed the existence of different kinds of intermolecular associations in the amorphous (liquid and glass) and crystalline (glacial and crystal) states. Obtaining information on the origin of the glacial state and on the relation between intermolecular associations and the glass transition mechanism requires detailed structural data in the different states of *n*-butanol. However, despite a recent diffraction study (Shmyt'ko *et al.*, 2010) there is a lack of structural information which would permit a detailed description of the hydrogen-bond associations in these states. To understand the mechanism of devitrification *via* the metastable glacial state, and the structural relation between the hydrogen-bond networks in the underlying stable crystal and the glacial state, the first step consists of obtaining a detailed structural description of the stable crystalline state.

The main subject of this paper is the structural elucidation of the crystalline phase of *n*-butanol, C_4H_9OH, from X-ray powder diffraction data. The intermolecular associations *via* hydrogen bonding will be analyzed in the light of Raman spectroscopy measurements performed in the intramolecular OH stretching region. The devitrification process will be described on the basis of X-ray diffraction and Raman data collected during an isothermal transformation of the supercooled liquid at 120 K, *i.e.* 2 K above the glass transition temperature T_g.

2. Experimental

2.1. X-ray diffraction

Data acquisition of the X-ray diffraction patterns in the different states of *n*-butanol was performed with an Inel curved position-sensitive gaseous detector (CPS 120). This detector consists of 8192 channels with an angular step approximately equal to 0.015°, covering the range 120° 2θ. The vertical Debye–Scherrer geometry, operating with a monochromatic Cu $K\alpha_1$ radiation (λ = 1.54056 Å) selected with an incident-beam curved-quartz monochromator, was used. The diffractometer was computer-controlled using the *Symphonix* software (Inel, 2007) and was calibrated using the attenuated direct beam at two-degree intervals. The minimum instrumental full width at half maximum (FWHM) was equal to $\sim$ 0.30°. *n*-Butanol was purchased at 99% purity from Aldrich and used without further purification. The liquid sample was filled into a Lindemann glass capillary (Ø = 0.7 mm), mounted at the center of the goniometer circle G3000 and rotated during the experiment around a horizontal axis in order to ensure proper averaging over the individual crystallites. An Oxford open gas-flow cryostat that keeps temperature fluctuations within $\pm$ 0.1 K was used to bring the sample in the crystalline state. The sample was firstly cooled from room temperature down to 110 K (8 K below T_g) at 6 K min^{-1}. The sample was then heated (6 K min^{-1}) and maintained at 120 K for isothermal ageing over the course of 24 h. During this isothermal ageing, the counting time for each diffraction pattern was 1 h. The transformation into the glacial state was complete after 8 h. The sample was further heated to 165 K (6 K min^{-1}) to obtain the overall crystallization, and then cooled down to 110 K for the data collection with an acquisition time of 24 h.

Table 1
Comparison of experimental Bragg peak positions from different diffraction patterns.

This work (110 K)		Shmyt'ko *et al.* (179 K)	
2θ (°)	Intensity	2θ (°)	Intensity
10.21	20.1	10.32	22.0
16.51	1.6	16.63	1.6
18.08	3.1	18.11	4.2
18.81	26.1	18.94	29.0
20.50	3.3	20.57	4.0
20.73	4.2	20.91	3.9
22.02	16.0	22.14	14.0
22.64	26.7	22.75	36.0
22.75	13.2	–	–
24.31	4.1	24.32	100.0
24.38	100.0	–	–
26.49	14.1	26.49	11.0
27.47	1.1	–	–
27.90	0.8	–	–
28.35	2.5	28.47	3.0

2.2. Raman spectroscopy

Liquid *n*-butanol was placed in a spherical Pyrex cell (Ø = 5 mm) and hermetically sealed. Raman spectra were collected on an XY Dilor spectrometer in back-scattering geometry, using the 514.5 nm light of a mixed argon–krypton coherent laser. The same Oxford temperature device and the same thermal history of the sample described for X-ray diffraction experiments were used for the analysis of the OH stretching region during the isothermal transformation of the supercooled liquid into the glacial state, and then in the crystalline state.

3. Results

3.1. Structural analysis of the stable crystalline state

For the determination of the lattice parameters of the stable state, the profile and the positions of 34 Bragg reflections with a 2θ angle lower than 43° were individually refined with the program *WinPLOTR* (Roisnel & Rodriguez-Carvajal, 2002). Their 2θ positions were introduced in the program *TREOR* (Werner *et al.*, 1985) and all these reflections were successfully indexed with a triclinic cell with the following parameters: a =

5.101 (1), b = 5.517 (1), c = 9.020 (1) Å, α = 79.1 (1), β = 75.8 (1), γ = 78.8 (1)°, V = 238.7 (2) Å^3. The values of the figures of merit are: $M(34)$ = 18, $F(34)$ = 40 (0.019, 45; Smith & Snyder, 1979; de Wolff, 1968). The same indexing of the Bragg peaks was obtained with the program *DICVOL* (Boultif & Louër, 2004). The parameters and the volume of the cell are different to the values found by Shmyt'ko (Shmyt'ko *et al.*, 2010) and yield a much improved figure of merit. In order to clarify the different indexings, the experimental angular positions of the Bragg peaks at low angles are reported in Table 1. There is a striking resemblance between the powder patterns. We reproduce the first seven Bragg reflections at lower angles with the same relative intensity. However, the previous study shows an intense single Bragg reflection at 22.75°, while two reflections are observed at 22.64 and 22.75° in this study. Fig. 1(*a*) clearly shows the splitting of the peaks which is due to the anisotropic dilatation of the sample between 110 and 179 K. Secondly, Table 1 and Fig. 1(*b*) show two very weak Bragg reflections at 27.47 and 27.90°, which are missing in the Shmyt'ko data.

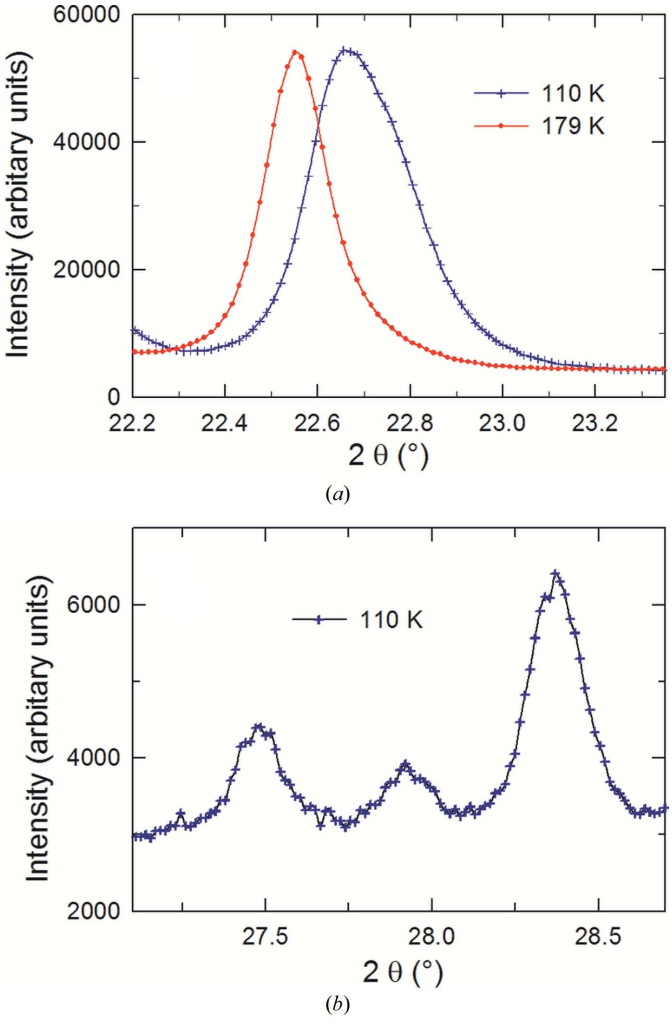

Figure 1
Details of the experimental diffraction pattern at 110 and 179 K. At 110 K, the Bragg peaks are at the angular positions: (*a*) 22.64 and 22.75°; (*b*) 27.47, 27.90 and 28.35°.

Table 2
Crystallographic data for *n*-butanol obtained after Rietveld refinements.

Crystal data	
Chemical formula	$C_4H_{10}O$
M_r	74.12
Crystal system, space group	Triclinic, $P1$
a, b, c (Å)	5.1014 (1), 5.5308 (1), 9.0323 (2)
α, β, γ (°)	79.027 (1), 75.758 (1), 78.826 (1)
V (Å^3)	239.59 (1)
Z	2
$F(000)$	84
D_x (Mg m^{-3})	1.027
Radiation type	Cu $K\alpha$, λ = 1.54056 Å
μ (mm^{-1})	0.56
Specimen shape, size (mm)	Cylinder, 0.7
Data collection	
Diffractometer	Inel CPS120
Specimen mounting	0.7 mm diameter Lindemann capillary
Data collection mode	Transmission
Scan method	Stationary detector
Step size (° 2θ)	0.015
2θ values (°)	$2\theta_{fixed}$ = 0.15–105.83
Refinement	
R-factors and goodness-of-fit (not corrected for background)	R_p = 0.037, R_{wp} = 0.050, R_{exp} = 0.017
No. of data points	7046
No. of parameters	74
No. of restraints	14
No. of contributing reflections	553
No of structural, profile parameters	29, 23
No of background points refined	22
No of bond length, bond angle constraints	8, 6

In order to confirm the parameters, the X-ray diffraction pattern was refined with the triclinic solution found by *TREOR* in the 2θ range 5.5–105.5° using the Le Bail fitting (Le Bail *et al.*, 1988) in the program *FullProf* (Rodriguez-Carvajal, 2010). In a first step, a pseudo-Voigt function with the same FWHM for the Gaussian and Lorentzian components is used to fit the Bragg peaks. This FWHM has a θ dependence according to Caglioti's law (Caglioti *et al.*, 1958). The asymmetry of the reflections was taken into account according to the Bérar and Baldinozzi function (Bérar & Baldinozzi, 1993). The background was determined with a linear interpolation between 22 points regularly distributed between 5.5 and 105.5°. At the end of the 'profile-matching' refinements, the profile reliability factors (corrected for background) are: R_p = 0.074, R_{wp} = 0.088. In a second step, the peak profiles were fitted with pseudo-Voigt functions using the Thompson–Cox–Hastings formalism (Thompson *et al.*, 1987). These functions take into account the experimental resolution and widening due to size and strain effects. The expression of the FWHM of the Gaussian and Lorentzian components is given elsewhere (Rodriguez-Carvajal & Roisnel, 2004). The instrumental resolution function was obtained through a Le Bail fit to the powder pattern of a standard compound ($Na_2Ca_3Al_2F_{14}$, NAC; Evain *et al.*, 1993) in the angular range 5.5–105.5° 2θ. To determine if the size and strain effects have to be considered as being isotropic or anisotropic, Le Bail refinements were performed for each combination of these effects. The best

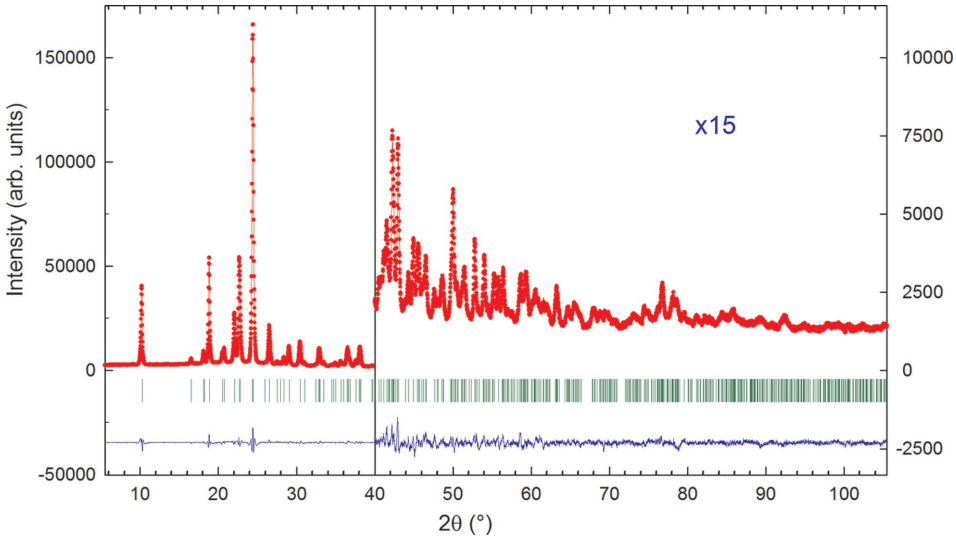

Figure 2
Final Rietveld plot of *n*-butanol. Observed data points are indicated by dots, the best-fit profile (upper trace) and the difference pattern (lower trace) are shown as solid lines. The vertical bars correspond to the positions of the Bragg peaks.

Table 3
Profile and structural parameters for *n*-butanol obtained after Rietveld refinements.

S400	2.77 (1)
S040	2.46 (15)
S004	1.09 (1)
S220	8.1 (3)
S022	−2.25 (9)
S211	6.0 (4)
S121	0.9 (3)
S112	1.1 (2)
S310	−7.4 (3)
S301	−2.45 (1)
S130	−1.4 (3)
S103	−1.19 (1)
S013	−0.84 (7)
S031	1.2 (2)
Asym1	0.067 (2)
Asym2	−0.0105 (4)
B_{iso} (Å^2)	1.49 (4)

improvement of the conventional agreement profile factors was obtained for anisotropic strains. The 45 refined parameters are as follows: the lattice parameters a, b, c, α, β and γ, the zero-shift, 14 strain parameters (Stephens, 1999; the strain parameter S202 and the Lorentzian–anisotropic strain mixing strain parameter were very close to zero and were kept fixed to zero in the last refinements), 2 parameters for the asymmetry of the Bragg peaks and 22 points to define the background. The agreement profile factors R_p and R_{wp} decrease to 0.065 and 0.077, respectively. The final lattice parameters were a = 5.1013 (1), b = 5.5320 (1), c = 9.0382 (2) Å, α = 79.008 (1), β = 75.719 (1), γ = 78.829 (1)° and V = 239.74 (1) Å^3.

In order to obtain a starting structural model, the 'parallel tempering' algorithm of the program *FOX* (Favre-Nicolin & Černý, 2002) was used. A molecule of butanol was built with standard bond lengths and angles and was introduced randomly into the cell. The 'relaxed restraints' option was used for the calculations, modifying the bond lengths and angles. The dihedral angles were treated as free parameters. At this stage, two space groups, $P\bar{1}$ and $P1$, were possible and were tried in *FOX*. The asymmetric unit contains one molecule in the first case and two molecules in the second case. The second solution with two independent molecules was appropriate because the agreement between the simulated pattern and the experimental one was much better with $P1$ than $P\bar{1}$. Thus, the corresponding atomic coordinates found by *FOX* were introduced in the program *FullProf* (Rodriguez-Carvajal, 2010) in order to perform Rietveld refinements. Soft restraints on the bond lengths and bond angles were applied. Standard deviations for restraint values in the final calculations were equal to 0.01 Å for bond lengths and 1.0° for bond angles.

For the Rietveld refinements, there are 74 adjustable parameters: (i) 45 parameters as described above; (ii) 29 structural parameters: the scale factor, one isotropic displacement parameter for C and O atoms, and 27 atomic coordinates of the non-H atoms. The H atoms were restrained to chemically reasonable positions in the Rietveld refinements. The position of the C1*a* atom was fixed to define the origin of the cell. No preferred orientations of the sample in the capillary could be shown in the Bragg peak refinements. The final conventional (corrected for background) Rietveld agreement factors are: R_p = 0.080, R_{wp} = 0.088, R_{exp} = 0.030 and χ^2 = 8.6. The mean-square deviations from the soft restraints are 0.014 Å for the bond lengths and 1.9° for the bond angles. The mean value of the electron-density synthesis is zero with a mean square deviation of 0.01 e Å^{-3}, the values of the highest peak and the deepest hole being equal to 0.02 and − 0.05 e Å^{-3}. The experimental and calculated diffraction patterns are shown in Fig. 2. Fig. 3 shows the unit cell drawn with *ORTEP*3 (Farrugia, 1997) and the numbering of the atoms. Crystallographic data, profile and structural parameters are given in Tables 2 and 3. Values of the bond lengths and bond angles are given in Table 4.[1]

The skeleton of each type of molecule is practically planar. The dihedral angles of Table 4 show that the O—C1—C2—C3 and C1—C2—C3—C4 sequences are practically in the *trans* conformation with respect to the C1—C2 and C2—C3 bonds, respectively. Characteristics of the hydrogen bonds are

[1] Supplementary data for this paper are available from the IUCr electronic archives (Reference: PS5021). Services for accessing these data are described at the back of the journal.

Table 4
Values of the bond lengths (Å) and angles (°) for *n*-butanol.

	Molecule *a*	Molecule *b*
C1—C2	1.518 (8)	1.536 (7)
C2—C3	1.515 (6)	1.516 (6)
C3—C4	1.503 (7)	1.540 (7)
C1—O	1.442 (6)	1.469 (5)
C2—C1—O	111.7 (4)	111.7 (4)
C1—C2—C3	112.5 (4)	111.2 (4)
C2—C3—C4	112.6 (4)	109.4 (4)
C1—C2—C3—C4	175.5 (4)	−175.4 (4)
C3—C2—C1—O	−176.1 (4)	173.7 (4)

reported in Table 5. The O atoms are involved in hydrogen bonds; each of them forms one donor and one acceptor bond. The hydrogen-bond network forms infinite chains in the [100] direction, as shown in Fig. 4(*a*). Fig. 4(*b*) shows the existence of C—H···O hydrogen bonds which are rarely observed in associated molecular liquids. In order to explore this possibility, we report below a Raman scattering investigation.

3.2. Raman spectroscopy

The Raman spectra in the C—H and O—H stretching regions are plotted in Figs. 5(*a*) and (*b*) in the supercooled liquid, glacial and crystalline states at 120 K. It is very noticeable that the C—H stretching spectrum in the crystalline state is dominated by a Raman band around 2885 cm^{-1} (framed in Fig. 5*a*), not existing in the liquid. In the glacial state a significant intensity is detected around 2885 cm^{-1} reflecting the presence of crystallized domains in the glacial state. The O—H stretching spectrum in the supercooled liquid state is composed of a broad double hump covering the 3100–

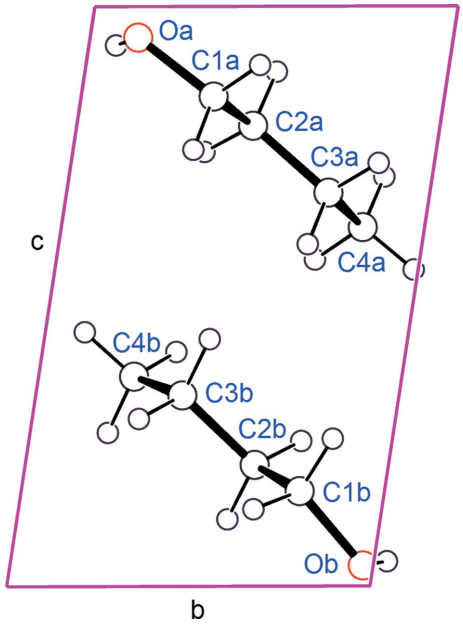

Figure 3
Projection of the unit cell along **a** * showing the atomic numbering of the molecules of *n*-butanol.

Table 5
Hydrogen-bonding geometry (Å, °) for *n*-butanol.

D—H···*A*	*D*—H	H···*A*	*D*···*A*	*D*—H···*A*
C2*a*—H2*a*′···O*b*^{i}	1.00	2.86	3.60	131.2
O*a*—HO*a*···O*b*^{ii}	0.85	2.03	2.78	146.3
O*b*—HO*b*···O*a*^{iii}	0.85	2.00	2.76	148.7

Symmetry codes: (i) $x-1, y, z+1$; (ii) $x-1, y-1, z+1$; (iii) $x, y+1, z-1$.

3500 cm^{-1} frequency range. The spectrum of the glacial state is composed of two broad bands at 3300 and 3400 cm^{-1}, emerging during the isothermal transformation, with a pronounced tailing on the low-frequency side of the 3300 cm^{-1} band. This tail can be considered as the residual intensity of the low-frequency contribution observed in the spectrum of the supercooled liquid, while the 3300 cm^{-1} band corresponds to the high-frequency hump in the supercooled liquid. It is clearly observed that both 3300 and 3400 cm^{-1} bands in the glacial state correspond to two sharp and intense

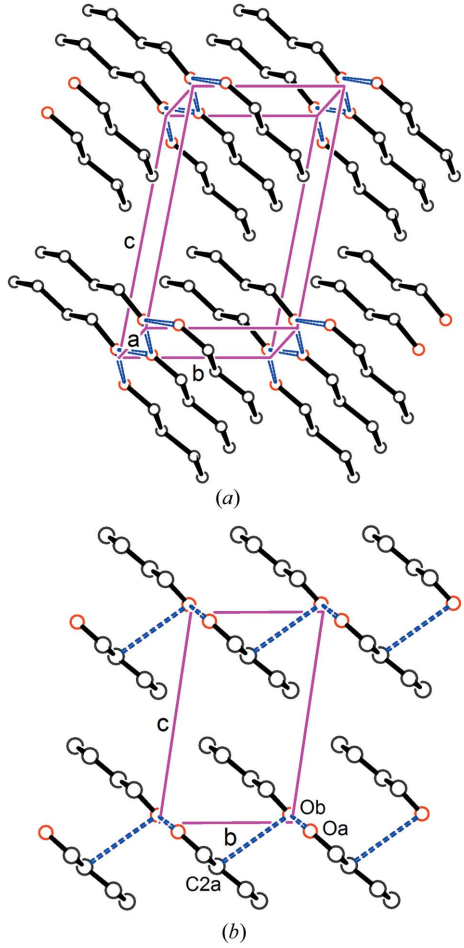

Figure 4
(*a*) Perspective drawing normal to the (100) plane of *n*-butanol. For the sake of clarity, H atoms and C—H···O hydrogen bonds have been omitted. Dashed lines correspond to O—H···O hydrogen bonds. (*b*) Projection of *n*-butanol along **a***. For the sake of clarity, H atoms have been omitted. Dashed lines correspond to both O—H···O and C—H···O hydrogen bonds.

bands in the crystal. The positions of both intense bands are determined from a fitting procedure using Gaussian functions, and their temperature dependence in the crystalline state is plotted in the inset of Fig. 5(*b*). The positive $\omega(T)$ slopes observed in the inset of Fig. 5(*b*) are the signatures of intramolecular OH stretching vibrations in O—H···O molecular associations (Finch & Lippincott, 1957). Consequently, Fig. 5(*b*) clearly shows the existence of two main kinds of hydrogen bonds in the crystal, corresponding to the 3300 and 3400 cm^{-1} bands, and a third minor class of hydrogen bond, related to the 3220 cm^{-1} band, which is predominant at low temperature in the supercooled liquid and the glass. Special attention was given to the C—H stretching spectrum, which is plotted in Fig. 6 at T = 100 and 175 K. The region in the box, localizing the intense band in the crystalline state, indicates that this band slightly shifts toward the high frequencies with increasing temperature. This behavior can be considered as the signature of C—H···O hydrogen bonds. The CH stretching spectrum was analyzed using a fitting procedure similar to that described in the analysis of the OH stretching bands above. The temperature dependence of the frequency of the 2885 cm^{-1} band, plotted in the inset of Fig. 6, is linear with a positive slope determined by a linear regression. The low value of this slope ($\sim$ 0.03 cm^{-1} K^{-1}) compared with those of both OH stretching bands ($\sim$ 0.16 and 0.29 cm^{-1} K^{-1}) reflects the existence of weak C—H···O hydrogen bonds, in agreement with the distance estimated from the structure refinement. It is noticeable that Raman spectroscopy shows that these types of hydrogen bonds are present in the crystal but not in the liquid and supercooled liquid states.

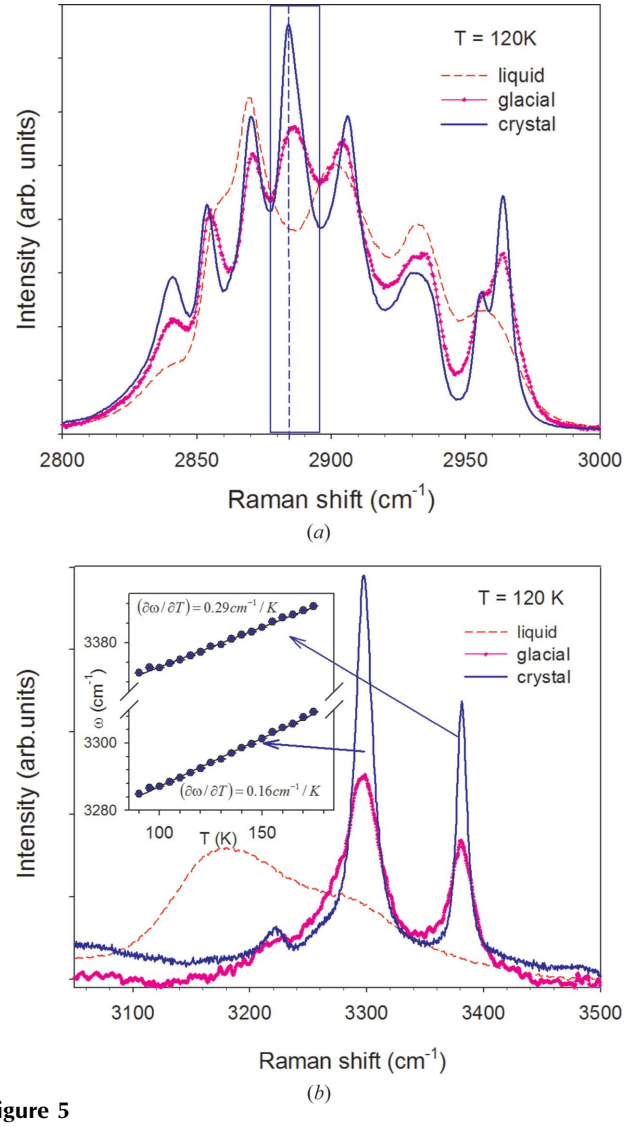

Figure 5
Raman spectra at 120 K in the undercooled liquid, glacial and crystalline states. (*a*) In the intramolecular CH stretching region, the rectangular box encloses the band existing in the crystal and not in the liquid. (*b*) In the OH stretching region, the temperature dependence of the wavenumber of both intense bands in the crystal is plotted in the inset.

3.3. Isothermal transformation of the supercooled liquid into the glacial state

The time evolution of the diffraction pattern of *n*-butanol during the isothermal transformation of the supercooled liquid at 120 K is plotted in Fig. 7. The X-ray diffraction pattern of the supercooled liquid is composed of a prepeak around 2θ = 10°, and a main peak around 2θ = 24°. The observation of an isolated peak at angles much lower than those attributed to the first intermolecular distances indicates an intermediate-range order in the supercooled liquid. It is recognized (Morineau & Alba-Simionesco, 1998) that the prepeak position reflects a repetitive distance, corresponding to a structural organization of $\sim$ 10.5 Å, extending over a distance of 18 Å, estimated from the width of the prepeak. Two main features can be observed during the isothermal transformation of liquid *n*-butanol. (i) The transformation of the prepeak into a relatively broad peak corresponding to the 001 Bragg peak of the crystal. (ii) The emergence of a relatively sharp peak from the main peak of the liquid, detected at

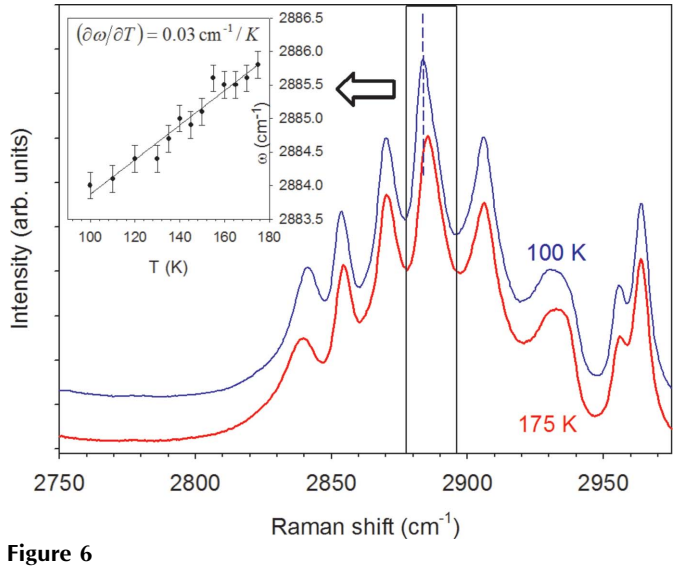

Figure 6
Raman spectra in the CH stretching region plotted at T = 100 and T = 175 K in the crystalline state. A clear shift of the most intense Raman band is clearly observed (within the rectangular box). The temperature dependence of the frequency is plotted in the inset.

$2\theta = 24^\circ$ and corresponding to the 012 Bragg peak of the crystal. The absence of other clear crystal features in the diffraction pattern of the glacial state prevents a rigorous microstructural analysis which must be performed on powder data covering the whole 2θ range. Nevertheless, microstructural information associated with the abortive crystallization can be obtained by analyzing separately the two crystalline signatures of the glacial state. The emergence of the broad peak from the large-angle side of the prepeak indicates that the intermediate-range order of the liquid develops in a restricted extension estimated to 200 Å in the direction perpendicular to the (001) plane, using the Scherrer formula. In contrast to this behavior the sharp band emerging from the main peak of the liquid reflects the preferential development of the long-range order in a larger extension (∼ 1350 Å) in the direction perpendicular to the (012) plane. Fig. 8 shows that this latter direction is perpendicular to the long molecular axis, and the growth of the sharp peak around $2\theta = 24^\circ$ suggests the stacking of molecular chains stabilized by C—H···O hydrogen bonds. The glacial state can be described as composed of microcrystallites characterized by a strong anisotropic geometry in agreement with the local arrangement described by Shmyt'ko (Shmyt'ko *et al.*, 2010). The average crystallite contains approximately 370 molecules in the direction perpendicular to the (012) plane and 46 molecules in the direction perpendicular to the (001) plane. These results are consistent with the existence strain effects in the crystalline phase, showing a strong anisotropic character. Fig. 9 shows the value of this strain in the *bc* plane of the lattice. The value of the strain ranges from 50.8×10^{-4} for the 001 reflection to 9.7×10^{-4} for $0\bar{1}1$ by way of 21.3×10^{-4} for 012. These features probably reflect a substantial disorder in the molecular layers of the glacial state, which prevents the overall crystallization.

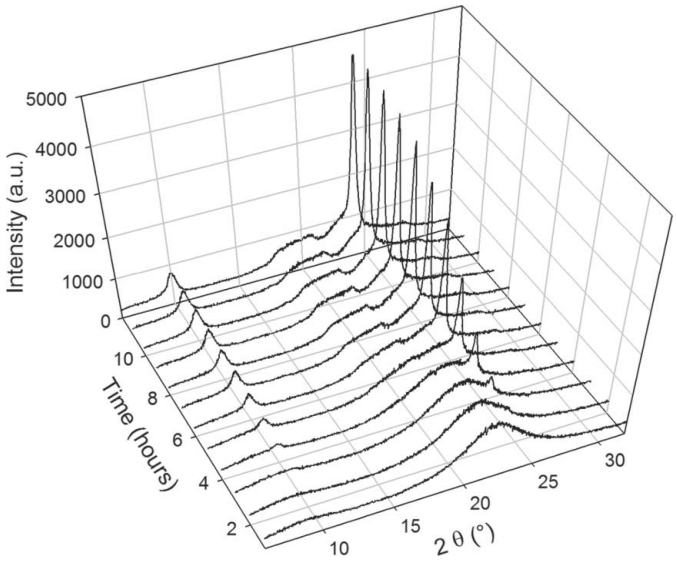

Figure 7
Three-dimensionnal plot of diffraction patterns during the isothermal transformations of the supercooled liquid at 120 K.

3.4. The origin of the abortive crystallization

Fig. 5(*b*) shows an intense low-wavenumber Raman band in the OH stretching region of the supercooled liquid state reflecting strong and predominant hydrogen bonding, not existing in the crystal. This broad Raman band largely disappears during the isothermal transformation, at the expense of two relatively sharp bands at wavenumbers distinctive of the hydrogen-bond network of the crystal. The OH stretching

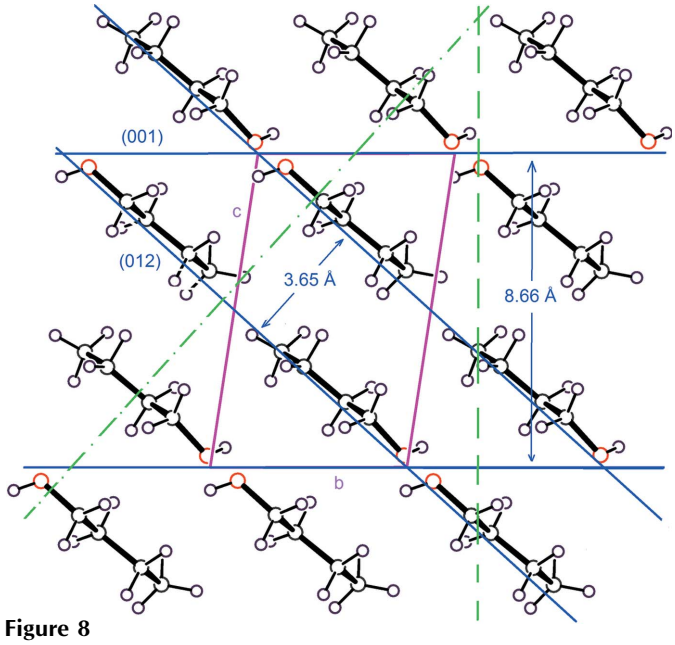

Figure 8
Projection of the structure along **a***. The long molecular axis lies in the (012) planes. The dashed and dash–dot straight lines denote the direction perpendicular to the (001) and (012) planes, respectively. The direction perpendicular to the (012) planes corresponds to the higher coherent length.

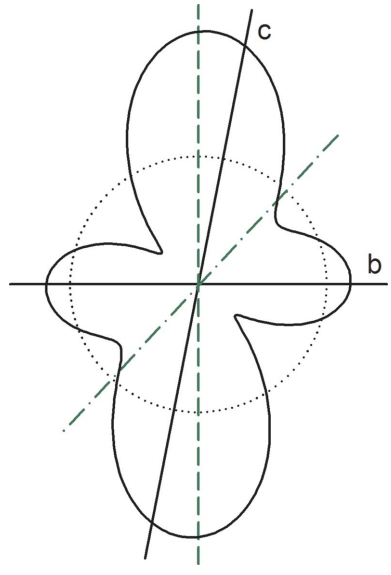

Figure 9
Anisotropic strain for different directions of the lattice of *n*-butanol in the *bc* plane. The dotted circle represents the average value of the strain: 26.2×10^{-4}. The dashed and dash–dot straight lines denote the direction perpendicular to the (001) and (012) planes, respectively.

spectrum in the glacial state reveals the coexistence of molecular associations distinctive of the crystal *via* both sharp bands around 3300 and 3400 cm^{-1}, and molecular associations which were predominant in the supercooled liquid *via* the pronounced tail on the low-wavenumber side of the 3300 cm^{-1} band. The strong character of the predominant hydrogen bond species existing in the supercooled liquid can be an argument to partly explain the abortive crystallization into the glacial state. A second argument could arise from the unusual C—H···O hydrogen bonds clearly shown by Raman spectroscopy (see Fig. 6), consistent with the present X-ray data. Fig. 5(*a*) shows that the distinctive band for these hydrogen bonds does not exist in the liquid, and it is known that the C—H group is rarely involved in hydrogen bonds under favorable conditions (Taylor & Kennard, 1982; Desiraju, 1991; Steiner & Saenger, 1992) concerning C···O distances (3.0–4.0 Å) and C—H···O angles (90–180°), in agreement with the present data reported in Table 5. The directional preferences of the C—H···O bonds are probably satisfied within the geometrical constraints of stronger O—H···O interactions (Desiraju, 1991). However, when they are sufficiently numerous these weak hydrogen bonds were found to play a crucial role in the formation of the molecular packing determining the crystal structure of various organic materials (Desiraju, 1991). In *n*-butanol these C—H···O bonds can be considered as an additional stabilizing force between molecules within chains and between molecular chains along the direction perpendicular to the (012) plane, necessary for the crystal cohesion. It is worth noting that the existence of C—H···O bonds was also demonstrated in the glacial (Derollez *et al.*, 2004) and crystalline (Hernandez *et al.*, 2002) states of triphenyl phosphite, widely investigated for similar and intriguing devitrification processes.

4. Conclusion

The present study gives the detailed organization of *n*-butanol molecules in the crystal. The structural description obtained in the present study is found to be in good agreement with that given by Shmyt'ko. However, the unit cell determined in the present study is different from that obtained by Shmyt'ko, probably because our data were collected at low temperature (120 K) compared with the temperature used by Shmyt'ko (179 K). As a consequence, the splitting of Bragg peaks and low-intensity peaks were considered in the present study and not in the analysis of Shmyt'ko. The isothermal transformation of the supercooled liquid into the glacial state can be interpreted as an abortive crystallization in microcrystallites characterized by a strong anisotropy, in agreement with previous studies (Wypych *et al.*, 2007; Shmyt'ko *et al.*, 2010). Molecular layers develop along the direction perpendicular to the (012) plane, while a substantial disorder exists inside the plane of the molecular layers. These features are probably inherent to the microstrains developing in the crystal and therefore are responsible for the broadening of Bragg peaks in the crystalline state. The origin of the glacial state was tentatively explained in terms of the competition of the strong O—H···O bonds predominant in the liquid and the weaker O—H···O bonds of the crystal. The coexistence of different types of molecular associations related to different O—H···O bond networks in the supercooled liquid state, coupled with an inherently small number of C—H···O interactions, possibly represent unfavorable conditions for crystallization.

References

Adam, G. & Gibbs, J. H. (1965). *J. Chem. Phys.* **43**, 139.
Bérar, J.-F. & Baldinozzi, G. (1993). *J. Appl. Cryst.* **26**, 128–129.
Bolshakov, B. & Dzhonson, A. (2005). *J. Non-Cryst. Solids*, **351**, 444–454.
Boultif, A. & Louër, D. (2004). *J. Appl. Cryst.* **37**, 724–731.
Caglioti, G., Paoletti, A. & Ricci, F. (1958). *Nucl. Instrum.* **3**, 223–228.
Cohen, I., Ha, A., Zhao, X., Lee, M. F. T., Strouse, M. J. & Kivelson, D. (1996). *J. Phys. Chem.* **100**, 8518.
Derollez, P., Hédoux, A., Guinet, Y., Lefebvre, J., Descamps, M. & Hernandez, O. (2006). *Z. Kristallogr.* **23**, 557–562.
Derollez, P., Hernandez, O., Hédoux, A., Guinet, Y., Masson, O., Lefebvre, J. & Descamps, M. (2004). *J. Mol. Struct.* **694**, 131–138.
Desiraju, G. R. (1991). *Acc. Chem. Res.* **24**, 290–296.
Evain, M., Deniard, P., Jouanneaux, A. & Brec, R. (1993). *J. Appl. Cryst.* **26**, 563–569.
Farrugia, L. J. (1997). *J. Appl. Cryst.* **30**, 565.
Favre-Nicolin, V. & Černý, R. (2002). *J. Appl. Cryst.* **35**, 734–743.
Finch, J. N. & Lippincott, E. R. (1957). *J. Phys. Chem.* **61**, 894–902.
Ha, A., Cohen, I., Zhao, X., Lee, M. & Kivelson, D. (1996). *J. Phys. Chem.* **100**, 1–4.
Hédoux, A., Guinet, Y., Derollez, P., Hernandez, O., Lefort, R. & Descamps, M. (2004). *Phys. Chem. Chem. Phys.* **6**, 3192–3199.
Hédoux, A., Guinet, Y., Derollez, P., Hernandez, O., Paccou, L. & Descamps, M. (2006). *J. Non-Cryst. Solids*, **352**, 4994–5000.
Hédoux, A., Guinet, Y. & Descamps, M. (1998). *Phys. Rev. B*, **58**, 31–34.
Hernandez, O., Hédoux, A., Lefebvre, J., Guinet, Y., Descamps, M., Papoular, R. & Masson, O. (2002). *J. Appl. Cryst.* **35**, 212–219.
Inel (2007). *Symphonix.* Inel Corporation, Artenay, France.
Kivelson, D., Kivelson, S. A., Zhao, X., Nussinov, Z. & Tarjus, G. (1995). *Physica A*, **219**, 27–38.
Kurita, R. & Tanaka, H. (2005). *J. Phys. Condens. Matter*, **17**, L293–L302.
Le Bail, A., Duroy, H. & Fourquet, J. (1988). *Mater. Res. Bull.* **23**, 447–452.
Mishima, O., Calvert, L. D. & Whalley, E. (1985). *Nature*, **314**, 76–78.
Morineau, D. & Alba-Simionesco, C. (1998). *J. Chem. Phys.* **109**, 8494–8503.
Rodriguez-Carvajal, J. (2010). *FullProf*, Version 4.80. ILL, Grenoble, France.
Rodriguez-Carvajal, J. & Roisnel, T. (2004). *WinPLOTR*, pp. 123–126. Trans Tech Publications, Zürich, Switzerland.
Roisnel, T. & Rodriguez-Carvajal, J. (2002). *Mater. Sci. Forum*, **378–381**, 118–123.
Shmyt'ko, I. M., Jiménez-Riobóo, R. J., Hassaine, M. & Ramos, M. A. (2010). *J. Phys. Condens. Matter*, **22**, 195102.
Smith, G. S. & Snyder, R. L. (1979). *J. Appl. Cryst.* **12**, 60–65.
Steiner, T. & Saenger, W. (1992). *J. Am. Chem. Soc.* **114**, 10146–10154.
Stephens, P. W. (1999). *J. Appl. Cryst.* **32**, 281–289.
Taylor, R. & Kennard, O. (1982). *J. Am. Chem. Soc.* **104**, 5063–5070.
Thompson, P., Cox, D. E. & Hastings, J. B. (1987). *J. Appl. Cryst.* **20**, 79–83.
Vahvaselkä, K. S., Serimaa, R. & Torkkeli, M. (1995). *J. Appl. Cryst.* **28**, 189–195.
Werner, P.-E., Eriksson, L. & Westdahl, M. (1985). *J. Appl. Cryst.* **18**, 367–370.
Wolff, P. M. de (1968). *J. Appl. Cryst.* **1**, 108–113.
Wypych, A., Guinet, Y. & Hédoux, A. (2007). *Phys. Rev. B*, **76**, 144202.